Flow regime study of Bubbling Fluidized bed gasifier & impact of fluidization velocity using Eulerian two fluid method

Mr. Mehul S. Parmar, Dr. Vishal N Singh, Dr. M.I. Shah
Department of Mechanical Engineering
A. D. Patel Institute of Technology, New Vallabh Vidhya Nagar, India.

Abstract

Fluidized bed characteristic of sand is present with Eulerian-Eulerian two fluid method. Commercial CFD software Fluent is used for simulation purpose and results are investigated with previous works. Cold flow model which is comparatively with gasification process is used for this fluidization behaviours study. Different flow regime studied and results are validated with experiment lab-scale results.

Keywords*: CFD, Fluidization, Eulerian-Eulerian, Flow regime, Granular Flow, Multiphase*

1.Introduction

Fluidization operations are used in many industries for various processes. As fluidization is complex behaviour it represents unsteady and transient behaviours of process. Qualitative idea of flow pattern is necessary for efficient and continuous operation of process. BFBG is widely used application which gives excellent temperature control, uniform temperature process, variety of fuels & lower tar formation. however, scale up of model is challenging task due to complicated reaction and mechanism [1]. Present study focus on the flow pattern predication with fluidization velocity and generating good model which give better predication for scale up process. At low velocity solid-volume fraction show high near the wall region while low at the centre. High gas velocity results in irregularity of particle concentration [2]. Relative velocities are large between particles in the centre region and maximum particle velocity achieved at the centre also particle velocity distribution is parabolic in nature is found out [3]. Velocity in riser is increased and leads to increase in outflow and it also affect the solid circulation rate. By increase in velocity total riser pressure drop encountered [4]. Simulation for 300 s and at nozzle velocity of 3.825 m/s with no-slip wall conditions rutile (particle diameter 69.5 µm & 4800 kg/m^3 density) and coke (particle diameter 355 µm & 1800 kg/m^3 density) particle move similar and their velocity difference termed as slip velocity. It is smaller in magnitude then rutile and coke particles individual velocity. It is observed that rutile particles are less quick or flow downward in riser comparing with coke particles [5].

Eulerian –Lagrangian method for investigate parameters like feeding rate in this they find that at inlet feed of mass 0.21 kg/h bed is converted into the bubbling bed [6]. In Eulerian-Eulerian method used for particle size 0.41 mm diameter and density of 1000 kg/m^3 carbon particles and simulate model in CFX and found out bubble at jet inlet formed as a single large bubble and causing bed expansion, considered as its unique feature. Bubble rise from ellipse shape and convert into round shape. Pressure distribution around bubble is high at top and low at bottom side. Bubbling produce uniform temperature profile around gasifier and effective heat transfer inside of gasifier. Some of particles are fall inside nozzle due to back flow also there is high oxygen rich area causing higher temperature at nozzle. Inside gasifier composition of gas distribution is non uniform and CO is concentrated around bubble and when bubble separate CO follow that bubble [7]. For solid hold up and circulation rate more important and stable circulation rate is good for enhanced heat transfer. after 30 sec of simulation it will take 5 s for fully developed flow and small bubble become larger as the bottom of the bed expand. Small bubbles are starched with other bubble and wall interaction. Solid circulation rate if high then particles are accumulating at lower part [8]. As velocity increase it may eventually show change in the bed expansion pattern and bubble phase loss its identity also rapid coalescence and break up make effect on flow

pattern [9]. For single gas phase and two granular phase assumption with maximum solid packing fraction of 0.68 and simulate bubble using second order discretization technique which are realistic in shape and behaviour. Bed was expanding from 0.2 m to 0.35 m and rutile particles having higher volume fraction and reasonable well mixed. High solid flux are below the bubbles [5]. At different co-ordinate system conclusion made that for bubbling fluidization in 2D geometry can predict good results and well agreements with 3D. Also cylindrical geometry takes more computational time than rectangular. Both 2D & 3D geometry having good agreements in results [10]. For 0.88 – 0.99 volume fraction, restitution coefficient of 0.95 predicts good results and in line with experimental data for given gasifier dimensions i.e. hydrodynamic behaviour in fluidization greatly influenced by restitution coefficient [2]. As restitution coefficient decrease particle-particle interaction becomes leas ideal and more fluctuating kinetic energy dissipated. Due to leas idea interaction mean particle diameter increase i.e. big particles are flow downward and small particles accumulate in upper region [3]. Effect of coefficient of restitution using kinetic theory of granular flow. When inelastic collision encountered then collisions becomes less ideals and particles are closely packing also when particle interaction becomes less ideal granular temperature decreases. Pressure distribution depends strongly on restitution coefficient as increase in energy dissipation then simulation show stronger pressure fluctuations i.e. more vigorous bubble are formed at e_{eff} = 0.73. When e = 0.97 interaction between particles becomes non-ideal and bubble are formed and when e = 1 segregation is much slower and interaction becomes ideal and no bubbles are present [11]. Restitution coefficient (e_{ss}) changes from 0.9 to 0.99 bed expansion change ~ 1.35 to ~ 1.45 at U = 0.38 m/s also at e_{ss} = 0.99 all drag models predicts vigorous bubbling also for e_{ss} = 0.9 results are not agreements with experimental data, i.e. sensitivity of system to e_{ss} is higher at $U < U_{mf}$ [12].

2.Mathematical Modeling

2.1 Volume Fraction Equation

Volume fractions represent the space occupied by each phase, and the laws of conservation of mass and momentum are satisfied by each phase individually. The derivation of the conservation equations can be obtained by ensemble averaging the local instantaneous balance for each of the phases or by using the mixture theory approach.

The Volume of Phase q, V_q is defined by

$$V_q = \int_0^v \alpha_q . dV \qquad 1$$

Where,

$$\sum_{q=1}^{n} \alpha_q = 1 \qquad 2$$

The effective density of phase q is calculated as

$$\hat{\rho}_q = \alpha_q . \rho_q \qquad 3$$

Where ρ_q is the physical density of phase q.

2.2 Conservation Equations

The motion of each phase is governed by respective mass, momentum and energy conservation equations [13,14].

Conservation of mass:

The Continuity equation for phase q is

$$\frac{\partial}{\partial t}(\alpha_q \rho_q) + \nabla . (\alpha_q \rho_q \vec{V}_q) = \sum_{p=1}^{n} (\dot{m}_{pq} - \dot{m}_{qp}) + S_q \qquad 4$$

The right-hand side of Equation (4.4) is zero. This is because the net mass transfer from one phase to another is zero and the source term is considered by default zero except for the constant user-defined boundary conditions. Thus we have the following continuity equations:

Gas phase:

$$\frac{\partial}{\partial t}(\alpha_g \rho_g) + \nabla.(\alpha_g \rho_g \vec{V}_g) = 0 \quad (5)$$

Solid phase:

$$\frac{\partial}{\partial t}(\alpha_s \rho_s) + \nabla.(\alpha_s \rho_s \vec{V}_s) = 0 \quad (6)$$

Conservation of momentum:

Newton's second law of motion states that the change in momentum equals the sum of forces on the domain. The momentum equation for phase q yields

$$\frac{\partial}{\partial t}(\alpha_q \rho_q \vec{V}_q) + \nabla.(\alpha_q \rho_q \vec{V}_q \vec{V}_q) = -\alpha_q \nabla.p + \nabla.\bar{\bar{\tau}}_q + \alpha_q \rho_q \vec{g} + \sum_{p=1}^{n}(\vec{R}_{pq} + \dot{m}_{pq}\vec{v}_{pq} - \dot{m}_{qp}\vec{V}_{qp}) + (\vec{F}_q + \vec{F}_{lift,q} + \vec{F}_{vm,q}) \quad (7)$$

Where $\bar{\bar{\tau}}_s$ is the q[th] phase stress-strain tensor

$$\bar{\bar{\tau}}_s = \alpha_s \mu_s (\nabla.\vec{V}_s + \nabla.\vec{V}_s^T) + \alpha_s (\lambda_s - \frac{2}{3}\mu_q)\nabla.\vec{V}_q \bar{\bar{I}} \quad (8)$$

$\vec{V}_{pq}$ is the interphase velocity. It is defined as follow. If $\dot{m}_{pq} > 0$ (i.e., phase p mass is being transferred to phase q), $\vec{V}_{pq} = \vec{V}_p$; If $\dot{m}_{pq} < 0$ (i.e., phase q mass is being transferred to phase p), $\vec{V}_{pq} = \vec{V}_q$. Similarly if $\dot{m}_{qp} > 0$, then $\vec{V}_{qp} = \vec{V}_q$; if $\dot{m}_{qp} < 0$, then $\vec{V}_{qp} = \vec{V}_p$ [15].

The $\vec{F}_{vm,s}$, virtual mass force and the $\vec{F}_{lift,s}$ lift force are considered zero by default. The equation 4.7 must be closed with appropriate expressions for the interphase force. The program uses a simple interaction term, in the following form:

$$\sum_{p=1}^{n}\vec{R}_{pq} = \sum_{p=1}^{n}K_{pq}(\vec{V}_p - \vec{V}_q) \quad (9)$$

Where K_{pq} ($=K_{qp}$) is the interphase momentum exchange coefficient. Thus considering the above and $\dot{m}_{pq} = \dot{m}_{qp} = 0$, the general equations take the following form for the gas and solid phases.

Gas phase:

$$\frac{\partial}{\partial t}(\alpha_g \rho_g \vec{V}_g) + \nabla.(\alpha_g \rho_g \vec{V}_g \vec{V}_g) = -\alpha_g \nabla.p + \nabla.\bar{\bar{\tau}}_g + \alpha_g \rho_g \vec{g} + K_{sl}(\vec{V}_g - \vec{V}_s) \quad (10)$$

Solid phase:

$$\frac{\partial}{\partial t}(\alpha_s \rho_s \vec{V}_s) + \nabla.(\alpha_s \rho_s \vec{V}_s \vec{V}_s) = -\alpha_s \nabla.p + \nabla.\bar{\bar{\tau}}_s + \alpha_s \rho_s \vec{g} + K_{sl}(\vec{V}_g - \vec{V}_s) \quad (11)$$

Conservation of Energy:

To describe the conservation of energy in Eulerian multiphase applications, a separate enthalpy equation is written for each phase:

$$\frac{\partial}{\partial t}(\alpha_q \rho_q h_q) + \nabla.(\alpha_q \rho_q \vec{u}_q h_q) = \alpha_q \frac{\partial P_q}{\partial t} + \bar{\bar{\tau}} : \nabla \vec{u}_q - \nabla \vec{q}_q + S_q + \sum_{p=1}^{n}(Q_{pq} + \dot{m}_{pq}h_{pq} - \dot{m}_{qp}h_{qp}) \quad (12)$$

2.3 Interphase Exchange Coefficient

Fluid-solid Exchange Coefficient

The fluid-solid exchange coefficient K_{sl} can be written in the following general form:

$$K_{sl} = \frac{\alpha_s \rho_s f}{\tau_s} \quad 13$$

Where **f** is defined differently for the different exchange coefficient model and $\tau_{s,}$ the particulate relaxation time is expressed as follows:

$$\tau_s = \frac{\rho_s d_s^2}{18\mu_l} \quad 14$$

Where d_s is the diameter of the particles of phase s. All definition of **f** includes a drag function (C_d)that is based on the relative Reynolds number (Re_s). It is this drag function that differs among the exchange co-efficient models.

In the present study, Gidaspow model has been used, which is the combination of Wen and Yu model and the Ergun equation When $\alpha_1 > 0.8$, the fluid solid exchange coefficient K_{sl} is of the following form

$$K_{sl} = \frac{3}{4} C_d \frac{\alpha_s \alpha_l \rho_l \left|\vec{V}_s - \vec{V}_l\right|}{d_s} \alpha_l^{-2.65} \quad 15$$

Where,

$$C_d = \frac{24}{\alpha_l \mathrm{Re}_s}\left[1 + 0.15(\alpha_l \mathrm{Re}_s)^{0.687}\right] \quad 16$$

Where Re_s is defined as

$$\mathrm{Re}_s = \frac{\rho_l d_s \left|\vec{V}_s - \vec{V}_l\right|}{\mu_l} \quad 17$$

1is 1th fluid phase, s is sth solid phase particles and d_s is the diameter of sth solid phase particles

When $\alpha_1 \le 0.8, K_{ls}$ is written as

$$K_{ls} = \frac{3(1+e_{ls})(\frac{\pi}{2} + C_{fr,ls}\frac{\pi^2}{8}).\alpha_s \rho_s \alpha_l \rho_l (d_l + d_s)^2 g_{0,ls} \left|\vec{V}_l - \vec{V}_s\right|}{2\pi(\rho_l d_l^3 + \rho_s d_s^3)} \quad 18$$

Solid-solid Exchange Coefficient

The symmetric Syamlal (1987) model is recommended for a pair of solids where the solid-solid exchange coefficient K_{ls} has the following form:

$$K_{ls} = \frac{3(1+e_{ls}) + (\frac{\pi}{2} + C_{fr,ls}\frac{\pi^2}{8})\alpha_s \rho_s \alpha_l \rho_l (d_l + d_s)^2 g_{0,ls}}{2\pi(\rho_l d_l^3 + \rho_s d_s^3)} \left|\vec{V}_s - \vec{V}_l\right| \quad 19$$

3. CFD MODEL OF BFBG

Reactor dimension used for fluidization study is 1.23 m height and 0.140 m diameter. Model geometry in three-dimensional as shown in Fig.1. Bubbling fluidized bed gasifier is fluidized by air is introduced from bottom and sand is initial at 0.3m static bed from distributor plate. Distributor plate having 1 mm diameter used and 30 Nos of holes are used in pattern for bubbling fluidization.

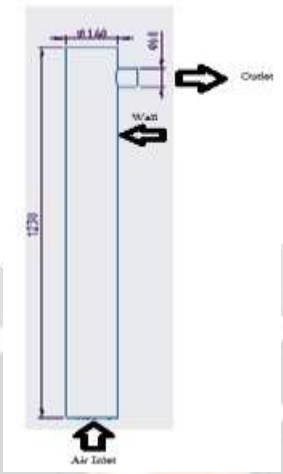

Fig. 1. Schemetic of Riser

4. Mesh Independent Test

In built Fluent package used for the meshing. Auto mesh with finer and medium options used with different element size for study independency of results from mesh. 15, 10, 8.5, 5 mm element size are used for the study. Fig.2 shows that reduction in element size below 5 mm to 2mm produce less effect on output results. And

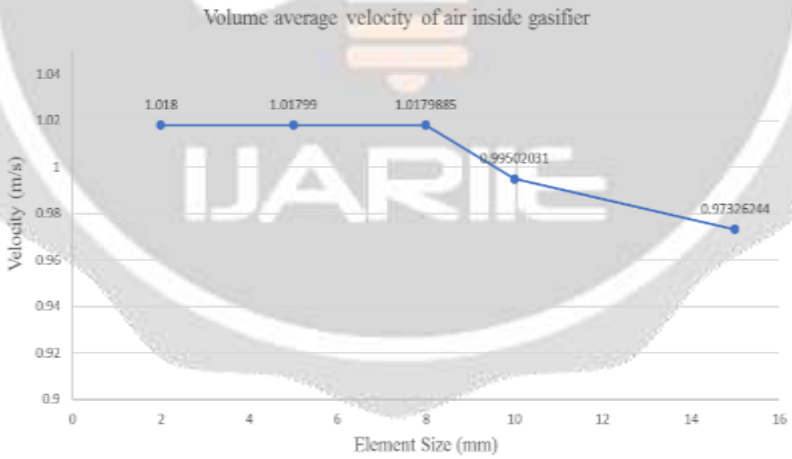

Fig. 2. Mesh Study for different element size and effect on results of volume average velocity inside gasifier.

5. Computational Setup

The reactor shown in Fig1. It's 3D model has been discretised. Boundary conditions at air inlet is velocity inlet and at outlet pressure outlet used. For wall no slip boundary condition used. Sand particle with initial diameter 0.271 mm is used for the simulation which falls into Geldart's B group. At the beginning reactor is filled up to 300mm height with sand particles.

6. Results

Different fluidization velocities are studied at minimum (0.02 m/s), Bubbling (0.25 m/s) & Turbulent (1.59 m/s) with particle size 0.271 & 2 mm. During simulation at minimum fluidization velocity high abrupt change occurred shown in Fig.3.

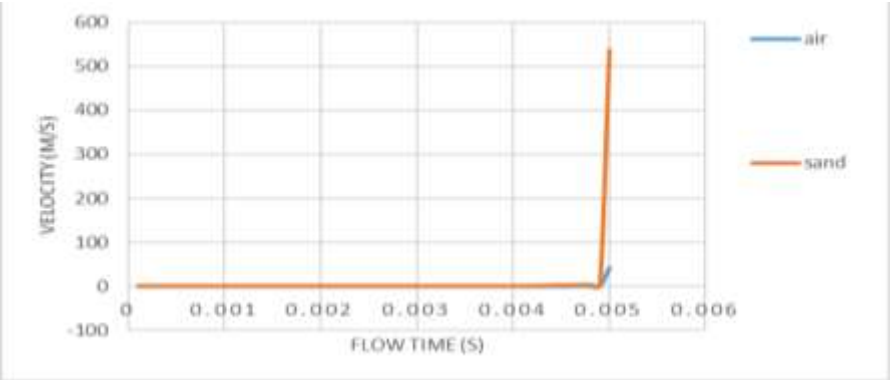

Fig. 3. Abrupt change in velocity at lower air flow rate.

At volume fraction of 0.6 and bubbling velocity bubble formation taken place. Large bubble formation begins at the 0.046 s around 0.126 s it reaches its maximum size and collapse in 0.225 s. So fast and vigorous bubbling taken place is shown in Fig.4.Absolute pressure inside gasifier is almost constant after initialization. Fluidization initial start with two picks and then turns into turbulent bed as shown in Fig.5.

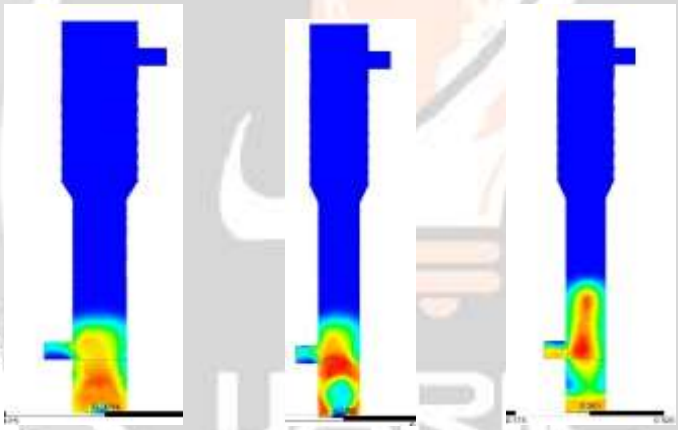

Fig. 4. Contour plot of volume fraction against time for sand at air velocity of 0.25m/s for initial static bed height of 0.3 m

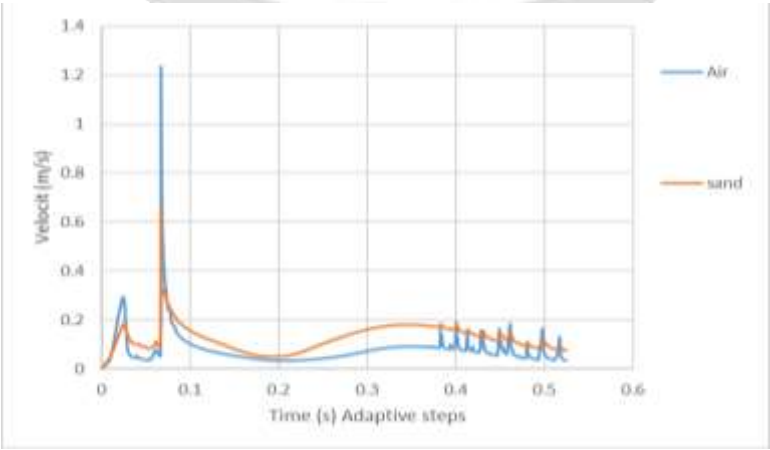

Fig. 5 Velocity variation inside gasifier

Static bed expansion taken place up to 10 sec significant time and then after not significant change observed. Bubbles are formed in distributed manor in whole domain. Also at low velocity mass accumulation start and that's why sufficient velocity required for continuous operation of bubbling behaviour and smooth working. Vigorous movement of solid particles are observed and near the wall downward velocity which represent fall down of particles near the wall side. Sand particles are try to collapse bubbles. Velocity variation of sand and air are shown in Fig.6.

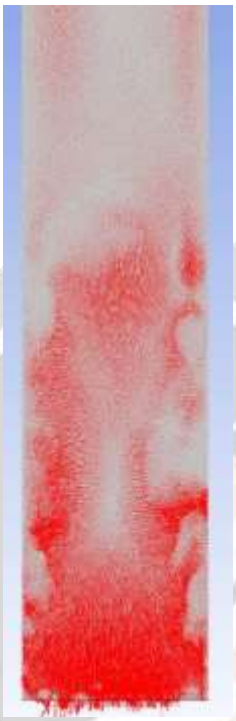

Fig. 6. Sand velocity vector

It also shows that at large velocity bed expansion is greater and turbulent in nature also smallest change of velocity change bed nature into other flow regime and alter the fluidization behaviour.

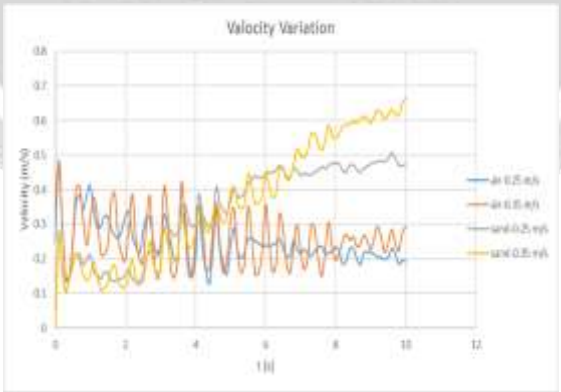

Fig. 7. Velocity variation time dependent

Axial pressure drop in fluidized bed varies from higher values at the bottom bed to the zero at the top of the bed column as in Fig 8.. Pressure is higher at the air inlet and gradually decrease and becomes zero at the outlet.

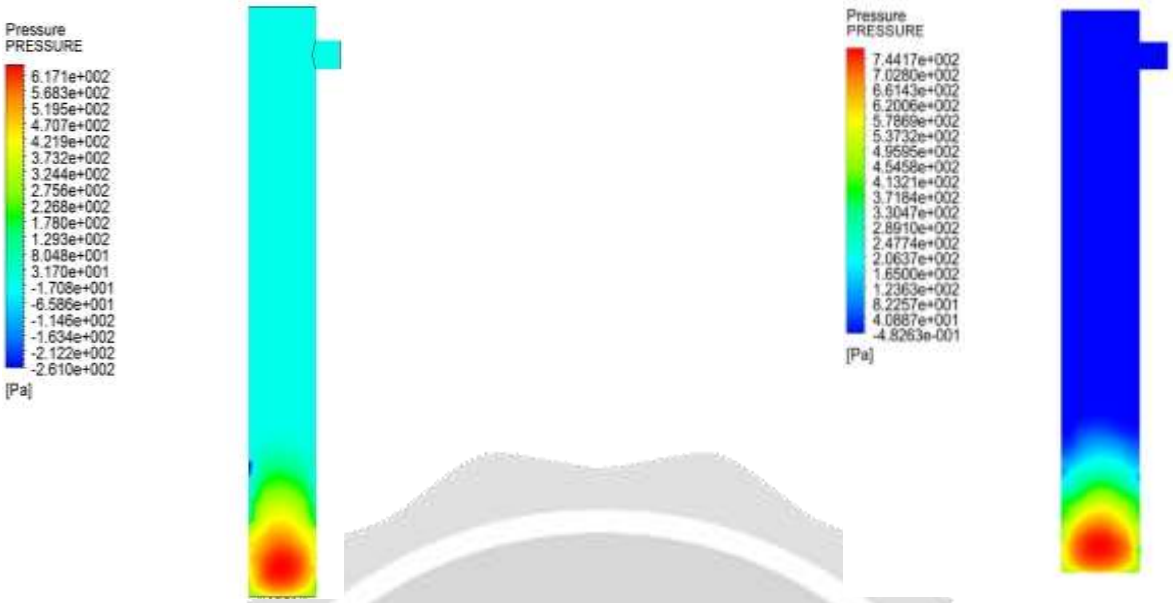

(a) 0.25 m/s velocity (b) 0.45 m/s velocity

Fig 8: contours of statics gauge pressure.

7. Conclusion

Bubbling generation take place at velocity of 0.25 m/s and 0.35 m/s. Vigorous bubble generated at e = 0.97 required 0.9 – 0.95 for smooth transition.0.2 mm Particle size is good for prediction of flow regime and bubbling fluidization. Geometry having great impact on fluidization and direct-scale up of model cannot be predicted.

▪ Nomenclature

d	Diameter(m)
F	Force(N)
V	Volume(m^3)
v	Velocity(m/s)
p	Pressure (Pa)
g	Acceleration due to gravity(m/s^2)
h	Specific Enthalpy (J/kg)
q	Heat Flux (J)
a	Speed of sound
M	Mash Number
N	Total Number of Phases
R	Rate of Reaction
T	Temperature(K)
K	Rate Constant
α	Volume Fraction
ρ	Density of Fluid(kg/m^3)
$\bar{\bar{\tau}}$	Stress-strain Tensor (Pa)
μ	Viscosity(kg/m s)
Φ	Angle of Internal Friction (deg)
η	Rate Exponent
S_q	Source Term(kg/s)
K_{pq}	Interphase Momentum Co-efficient
K_{ls}	The Fluid-Solid and Solid-Solid Exchange Coefficient

I_{2D}	Second Invariant of the Deviatoric Stress Tensor (Pa)
τ_p	Particulate Relaxation Time (s)
Re	Reynolds Number
e_{gs}, e_{ss}	Coefficient of Restitution
$g_{o,ls}$	Radial Distribution Co-efficient
C_D	Drag Co-efficient (kg/m^3.s)
$C_{fr,ls}$	Coefficient of friction Between the 1th and Sth Solid Phase Particles
Θ_s	Solid Phase Granular Temperature (m^2/s^2)
g_0	Radial Distribution Function
μ_s	Solid Shear Viscosity (kg/m.s)
$\mu_{s,col}$	Collision Viscosity(kg/m.s)
$\mu_{s,kin}$	Kinetic Viscosity(kg/m.s)
$\mu_{s,fr}$	Frictional Viscosity(kg/m.s)
λ_s	Bulk Viscosity(kg/m.s)
K_{Θ_s}	Diffusion Co-efficient(kg/m.s)
Υ_{Θ_s}	Collisional Dissipation of Energy(J)
Φ_{ls}	Energy exchange between 1th and Sth solid phase (J)
$\vec{U}_q$	Phase-weighted Velocity(m/s)
ε_q	Dissipation Rate (m^{-2}/s^{-3})
$\Pi_{k_q} = \Pi_{\varepsilon_q}$	Influence of Dispersed Phase on Continuous phase q
$G_{k,q}$	Turbulence Kinetic Energy(m^2/s^2)
$\tau_{F,pq}$	Characteristic Relaxation Time(s)
Γ_ϕ	Diffusion coefficient for ϕ
∇	Gradient
G_k	Generation of Turbulence Kinetic Energy due to the Mean Velocity Gradients
G_b	Generation of Turbulence Kinetic Energy due to Buoyancy
$C_{i\varepsilon}$	Constants
Y_M	Contribution of the Fluctuating Dilatation in Compressible Turbulence to the overall Dissipation Rate
σ_k	Turbulent Prandtl Number For k
σ_ε	Turbulent Prandtl Number For ε
S_k, S_ε	User Defined Source terms
β	Coefficient of Thermal Expansion
P_{rt}	Turbulent Prandtl Number
Y_i	Mass Fraction of Species
ν'	Stoichiometric coefficient of reactant
ν''	Stoichiometric coefficient of product

▪ References

[1] Basu Prabir., Biomass Gasification, Pyrolysis and Torrefaction Practical Design and Theory, 2nd ed., 2013.
[2] Jinsen Gao et al. 2009, CFD Modeling and Validation of the Turbulent Fluidized Bed of FCC Particles, Particle technology and fluidization, AIChE Vol 55, No 7,1680-1694.
[3] Lu Huilin et al., 2003, Hydrodynamics of binary fluidization in a riser: CFD simulation using two granular temperatures. China, Che. Eng. Sci. 58, 3777-3792.
[4] Siddhartha Shrestha et al., 2016, Hydrodynamic properties of a cold model of dual fluidized bed gasifier: A modeling and experimental investigation. Malaysia, Che. Eng. Res. & Des. 109, 791-805
[5] Scott Cooper et al., 2005, CFD simulation of particle mixing in a binary fluidized bed. USA, Powder Technology 151, 27-36.
[6] Michael Oevermann et al., 2009, Euler- Lagrange/DEM simulation of wood gasification in bubbling fluidized bed reactor. Germany, Particuology 7, 307-316.
[7] Kun Gao et al., 2006, Bubble dynamics and its effect on the performance of a jet fluidised bed gasifier simulated using CFD. Fuel 85, 1221-1231.
[8] Thanh D.B. Nguyen et al., 2012, CFD simulation with experiments in a dual circulating fluidized bed gasifier. South Korea, Comp. & Che. Eng. 36, 48-56.
[9] Ravindra Kumar et al., 2012, CFD analysis of circulating fluidized bed combustion. India, ESTIJ, vol 2, No 1, 163-174.
[10] Nan Xie et al., 2008, Effects of using two- versus three-dimensional computational modeling o fluidized beds Part I, hydrodynamics, USA, Powder Technology, Vol 182, 1-13.
[11] M.J.V. Goldschmidt et al., 2001, Hydrodynamic modelling of dense gas-fluidised beds using the kinetic theory of granular flow: effect of coefficient of restitution on bed dynamics. Netherlands, Che. Eng. Sci. 56, 571-578.
[12] Fariborz Taghipour et al. (2005), Experimental and computational study of gas–solid fluidized bed hydrodynamics, Che. Eng. Sci.60,6857-6867.
[13] "ANSYS Fluent 18.0", User's guide (2017).
[14] "ANSYS Fluent 18.0", Theory guide (2017)
[15] Kunii D. and Levenspiel O., "Fluidization Engineering", Second Ed., Butterworth Heinemann, Boston, 1991.